Journal of Hydrology 529 (2015) 120–133

Contents lists available at ScienceDirect

Journal of Hydrology

journal homepage: www.elsevier.com/locate/jhydrol

A groundwater conceptual model and karst-related carbon sink for a glacierized alpine karst aquifer, Southwestern China

Cheng Zeng [a], Zaihua Liu [a,*], Jianwen Yang [b], Rui Yang [a]

[a] State Key Laboratory of Environmental Geochemistry, Institute of Geochemistry, Chinese Academy of Sciences, Guiyang 550002, China
[b] Department of Earth and Environmental Sciences, University of Windsor, Windsor, ON N9B 3P4, Canada

ARTICLE INFO

Article history:
Received 24 January 2015
Received in revised form 10 July 2015
Accepted 18 July 2015
Available online 23 July 2015
This manuscript was handled by Laurent Charlet, Editor-in-Chief, with the assistance of Nico Goldscheider, Associate Editor

Keywords:
Jade Dragon Snow Mountain
Glacierized alpine karst aquifer
Conceptual hydrogeological model
Hydrochemistry
Stable isotopes
Karst-related atmospheric CO_2 sink

SUMMARY

In the Jade Dragon Snow Mountain (JDSM) region, Yunnan Province, SW China, an extensive hydrochemical and stable isotopic study of a glacierized alpine karst aquifer was conducted during the period, 2011–2014. The objectives of the study were: first, to establish a conceptual hydrogeological model of the karst groundwater system; second, to estimate the proportion of extra glacier melt water infiltrating the karst aquifer that is being induced by the regional climate warming; third, to calculate the karst-related flux of carbon into the karst aquifer. Knowledge of the local hydrogeological background from previous work was the starting point of the hydrochemical and stable isotopic study. Some representative spring waters and recharge waters (i.e. glacier melt water and rainwater) were investigated both spatially and temporally by hydrochemical and isotopic techniques, including analysis of major and some minor ions and O and H stable isotopes. A conceptual hydrogeological model of a fracture-diffuse flow karst groundwater aquifer was proposed. The proportion of glacier melt water infiltrating into the karst aquifer was estimated by using the karst spring as a natural pluviometer, and with stable isotope analysis. Results show that (1) the JDSM karst aquifer is a diffuse flow system; (2) it has a number of discharge areas, and the Jinsha River is the karst drainage base level; (3) the proportion of the glacier melt water penetrating the karst aquifer is 29%; and (4) the karst-related carbon sink is 26.67 ± 3.44 t km^{-2} a^{-1} (as CO_2), which is lower than that in non-glacierized karst aquifers but over ten times larger than the carbon sink flux from silicate weathering in non-karst areas, showing the control of both climate and lithology on the rock weathering-related carbon sink and the significance of carbonate weathering in the global carbon cycle.

1. Introduction

According to the Fifth Assessment Report of the Intergovernmental Panel on Climate Change (IPCC), the globally averaged surface temperature data show a warming of 0.85 [0.65–1.06] °C over the period 1880–2012 due to the increase of the atmospheric concentration of CO_2 because of fossil fuel emissions and net land use change emissions. Study of the global carbon cycle has become the focus of much global climate change research as a consequence. Warming of the climate is producing many changes, such as warming of atmosphere and ocean, diminution of amounts of snow and ice, and rise of sea level. The average rate of ice loss from glaciers around the world shows a remarkable accelerating trend (IPCC, 2013). The cryosphere is sensitive to the climate change, especially in temperate glacier-covered mountainous regions. In the Alps and Central Asia, the areas of glacier coverage have been showing strong diminishing trends (Kääb et al., 2002; Khromova et al., 2003; Paul et al., 2004a,b).

Lijiang is a famous international tourist city in NW Yunnan Province, China. However, a shortage of water has been more and more severe recently because of the rapid expansion of tourism. The temperate mountain glacier on the top of Jade Dragon Snow Mountain (JDSM), which is perhaps one of the most important water resources in the region, has been shrinking rapidly due to local climate change (He and Gu, 2003; He et al., 2003; Zeng et al., 2013). JDSM is located in a carbonate rock region. According to Hartmann et al. (2014), in many karst regions in the world, there will be an obvious decrease of precipitation and an increase in temperature over the next decades, and mountains are sentinels of climate change. As a result, the water supply problem is acute and getting worse in the JDSM region. Therefore, it is clearly essential to study the overall hydrogeological situation there.

The carbonate dissolution process, the global water cycle and the photosynthetic uptake of DIC (dissolved inorganic carbon)

* Corresponding author. Tel.: +86 851 85895263.
E-mail address: liuzaihua@vip.gyig.ac.cn (Z. Liu).

http://dx.doi.org/10.1016/j.jhydrol.2015.07.027
0022-1694/

constitute an important sink for atmospheric CO_2 (Liu et al., 2010). Freshwater storage in glaciers, ice caps and permanent snow is estimated to account for more than half (68.7%) of the total freshwater on the Earth (Gleick, 1996). The enhanced amounts of glacier melt water in karst regions released by climate warming participate in the water cycle and probably increase the karst-related carbon sink flux (Zeng et al., 2011, 2012). There are clear relationships between atmospheric CO_2, chemical weathering and glaciers (Gibbs and Kump, 1994; Sharp et al., 1995; Anderson and Drever, 1997. Krawczyk and Bartoszewski, 2008; Maher and Chamberlain, 2014). However, most previous studies have been conducted in glacierized non-karst regions. Zeng et al. (2012) reported on the atmospheric CO_2 sink under climate warming at the Glarey spring in the Tsanfleuron glacierized karst area in the Swiss Alps. The Tsanfleuron alpine karst is a typical conduit-dominated karst aquifer system (Gremaud et al., 2009). It shows remarkable diurnal and seasonal hydrochemical variations chiefly controlled by air temperature which influences the aquifer recharge by ice and snowmelt (Zeng et al., 2012).

The Jade Dragon Snow Mountain (JDSM) glacier is a typical temperate mountain glacier. It has attracted much scientific attention, with previous studies being focused on stable isotopic variations in rainwater, snow and glacier meltwater, and river water, and on ionic compositions and $\delta^{18}O$ in the shallow firn profile (He et al., 2002, 2006; Pang et al., 2005, 2006; Pang et al., 2007; Zhu et al., 2013). In particular, there is a primary study of the geochemistry and chemical exchange between groundwater and surface water in the Lijiang glacial basin by stable oxygen isotope and major ion analysis (Pu et al., 2013a). However, until now, little light has been shed on the hydrogeological conditions in this glacierized alpine karst aquifer, the groundwater conceptual model and the karst-related carbon sink in the aquifer.

Therefore, we conducted an extensive study of the JDSM alpine karst aquifer. The primary study objectives are: (1) to establish a conceptual groundwater model of the aquifer by use of hydrochemical and isotopic data; (2) to estimate the proportion of glacier meltwater stimulated by climate warming that is infiltrating into the underlying karst aquifer; (3) to calculate the karst-related carbon sink (flux) into the aquifer.

2. Description of Jade Dragon Snow Mountain (JDSM)

Jade Dragon Snow Mountain (JDSM) is located in Lijiang district, Yunnan Province, SW China (Fig. 1). It is a massif 35 km in length from north to south and 18 km in width from east to west, in the southeastern margin of the Qinghai-Tibet plateau and in the northwest of Lijiang Basin (Fig. 1). It belongs to the alpine – gorge landform suite. Its highest peak is Shanzidou (5596 m a.s.l).

JDSM is the southernmost glacierized mountain on the Eurasian continent. In 1957 there were 19 temperate mountain glaciers on its top with a total area of 11.6 km^2. However, in 2009 there were just 13 glaciers remaining, with only a total area of 4.42 km^2. Substantial glacier retreat was obvious (Du et al., 2013).

The study area is characterized by a monsoon climate with marked wet and dry seasons, (Fig. 2). More than 80% of the annual precipitation occurs during the wet season from June to September. The annual average precipitation is 957.2 mm, and the mean air temperature is 12.8 °C in Lijiang (Zeng et al., 2013). The annual mean air temperature near the Baishui No. 1 glacier tongue (4300 m in altitude) is 2.1 °C (Xin et al., 2013).

3. Hydrogeological background of the JDSM region

An extensive hydrogeological survey of the JDSM region was conducted after analysis of previous work (Figs. 3–5). The hydrogeological investigation included spring and glacier surveys, precipitation and snow and ice sample collection. The investigated springs include Jinsha-Daju (1), Changshui (2), Baishui (3), Heishui (4), Yuzhuqingtian (5) and Yushuizhai (6) Springs (Figs. 1, 3 and 5). Snow and ice specimens were collected from Baishui No. 1 Glacier (Fig. 3).

The principal bedrock of the snow mountain massif (Fig. 3) is carbonate, including marble and crystalline limestone of the upper Sanxiangu Formation (middle Devonian D_2s^2), marble and dolomitic marble of upper Devonian (D_3), and Carboniferous and lower Permian (P_1) crystalline limestone and marbles. These pure, intensively fractured carbonate rocks form an important aquifer for the water supply of Lijiang City. An undated sericite schist (M) occurs to the west of the snow mountain and forms a western aquiclude. Other aquicludes are created by dense, massive amygdaloidal basalts and volcanic tuffs of Permian age (P_β) on the southwest and northeast flanks of the mountain (Fig. 5A).

There is an active fault (the eastern JDSM Fault) along the eastern foothills that strikes approximately N–S and dips steeply eastwards. This fault presents a flow barrier because it is filled with fault gouge. There is a Quaternary moraine of carbonate gravel overlying the eastern basalt footwall of the fault, forming a porous aquifer in the unconsolidated sediment. The karst water in the JDSM alpine carbonate aquifer recharges this eastern morainic aquifer laterally in the form of subsurface flow.

The Jinsha River flows northeast through the northwestern part of the snow mountain, in Hutiaoxia Gorge (Leaping Tiger Gorge). Around 15 km in length, the gorge passes between Jade Dragon Snow Mountain and Haba Snow Mountain (Fig. 1). With a maximum depth of approximately 3790 m from mountain peak to river, the gorge is one of the deepest and most spectacular river canyons in the world.

Jade Dragon Snow Mountain and Haba Snow Mountain on the two sides of the Hutiaoxia Gorge belong to the same carbonate rock mass. There is no major fracture between the two Snow Mountains, so that the gorge is the result of an antecedent river which has been downcutting during tectonic uplift (Ming et al., 2007; Kong et al., 2010).

As mentioned, the lithology of the massif is dominated by marble which usually functions as an important aquifer. According to a tracer test in a nearby alpine-gorge area (Jinping District, western Sichuan Province), the marble aquifer is characterized by diffuse-flow in dense joints, sparse crannies and few karst conduits, and by a very thick unsaturated zone. The large difference in altitude between the recharge area and discharge area has caused the regional deep water flow system (Huang et al., 1995; Ma et al., 2006).

During our field hydrogeological survey, no karst caves were found in the JDSM area. There are a few dam foundation exploration adits in northwest part along the Jinsha River. Dripping water can be observed in a 150 m adit drilled in the carbonate unsaturated zone near Jinsha-Daju spring (Fig. 5G), showing the characteristics of diffuse flow. There are a great number of karst fractures (e.g., dissolutionally enlarged fractures and crushed rocks) in the carbonate bedrock underlying the JDSM glaciers (Fig. 5D and E). Most precipitation and glacier melt water recharges the alpine aquifer directly through them. Therefore, there are few surface streams in the study area.

The elevation of the northern Lijiang Basin is about 2700 m, and the Jinsha River at 1620 m in Hutiaoxia Gorge is the lowest modern karst drainage base level for the glacierized alpine karst aquifer. Karst development in the carbonate aquifer has always lagged behind the relatively rapid entrenchment of the Jinsha River because of the combination of isostatic rebound and fluvial entrenchment in the Jade-Dragon-Haba carbonate block since the

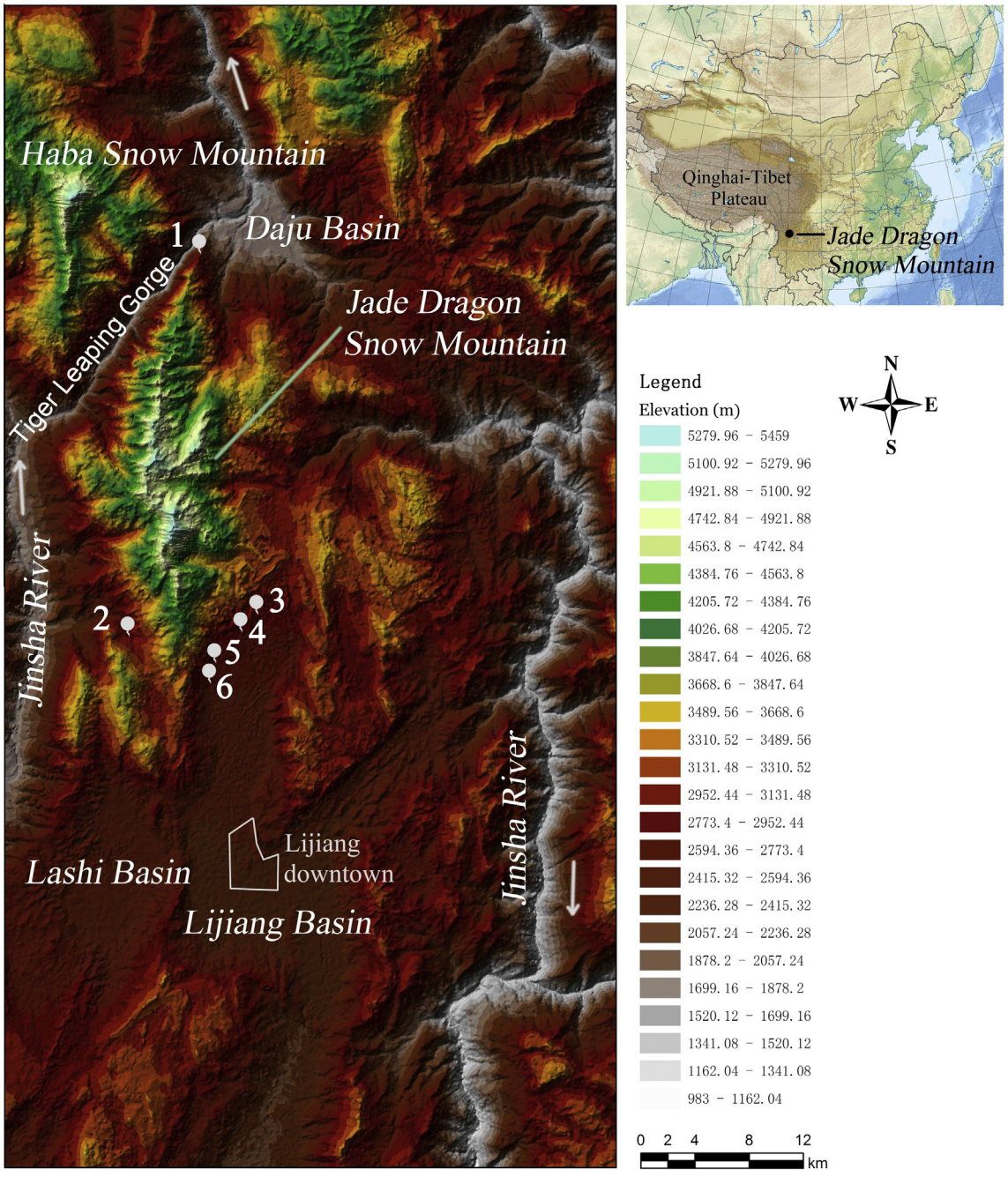

Fig. 1. Location of Jade Dragon Snow Mountain in China and its digital elevation model. Springs: 1 – Jinsha-Daju Spring; 2 – Changshui Spring; 3 – Baishui Spring; 4 – Heishui Spring; 5 – Yuzhuqingtian Spring; 6 – Yushuizhai Spring.

Late Cenozoic (Shi et al., 2008). It is supposed that there is a karst ground water divide between Jinsha River and the Lijiang Basin located within the snow mountain (Fig. 4).

Southeast of the snow mountain, the Lijiang Basin is overlain by 0–300 m of Quaternary unconsolidated glacial till (Q_{gl}) with high permeability. The low permeability amygdaloidal basalt (P_2^{β}) underlies the glacial till. The karst water recharges this Lijiang Basin morainic aquifer laterally, as noted.

The karst aquifer has at least two discharge areas, one into the Jinsha River at Jinsha-Daju Spring (No. 1 at 1620 m; Fig. 5H), the other into the Lijiang Basin unconsolidated aquifer, where several springs (Nos. 2–6) appear at the southeastern and southern margins of the snow mountain at elevations from 2741 m to 2899 m (Figs. 1, 3 and 5).

4. Methods of hydrochemical and stable isotopic measurement and calculation of the karst-related carbon sink

In order to establish the groundwater recharge-runoff-discharge pattern, calculate the proportion of glacier melt-water penetrating into the aquifer and the karst-related carbon sink in the JDSM, hydrochemical and stable isotopic measurements were used in the study. There was *in-situ* titration in the field and major ion analysis in the laboratory. CO_2 partial pressure and calcite saturation index of karst water were calculated. The stable isotopic measurements were of $\delta^{18}O$, $\delta^{2}H$ and $\delta^{13}C_{DIC}$. Most of the spring water samples (sampling locations in Fig. 3) were collected at intervals of two months between August 2011 and December 2013. The carbonate chemistry of karst water is highly sensitive

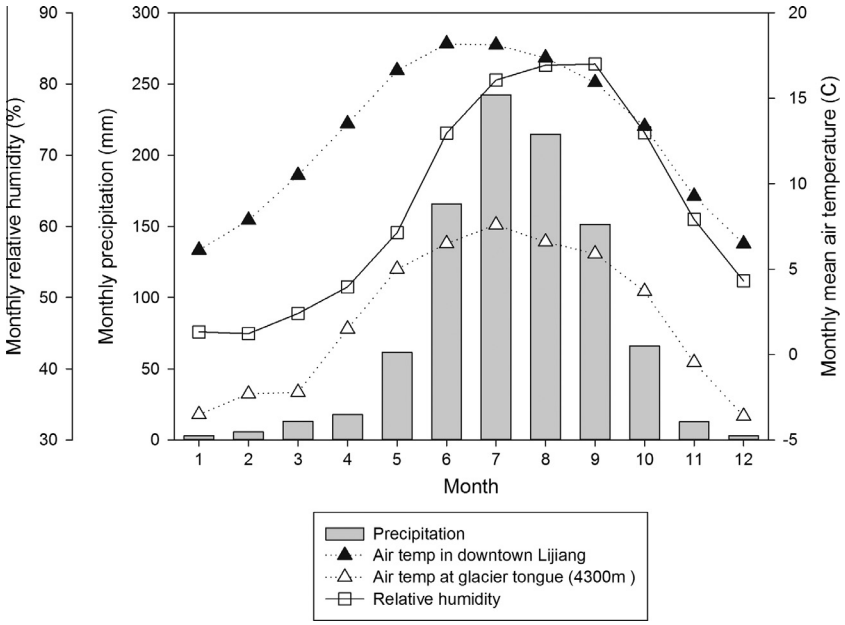

Fig. 2. Statistics of precipitation, air temperature and relative humidity in Lijiang (from 1951 to 2012).

to atmospheric conditions, so the basic physicochemical parameters (i.e. water temperature, pH and bicarbonate concentration) of groundwater were measured *in situ* as soon as the water samples were collected (per Fetter, 1994).

4.1. In-situ titration and major ions analysis in laboratory

Bicarbonate and Ca^{2+} concentrations of water were titrated *in situ* with an Aquamerck alkalinity test kit and the hardness test kit (Zolotov et al., 2002; Banks and Frengstad, 2006; Liu et al., 2007), with an accuracy of 0.05 mmol/L and 1 mg/L respectively. Two sets of 60 ml water samples were transferred in acid-washed hydroplastic bottles for chemical analysis of cations and anions within two weeks, after filtering through 0.45 μm Millipore filters. The cation test samples were acidified to pH < 2.0 with concentrated nitric acid to prevent complexation and precipitation.

In the laboratory, cation concentrations of Na^+, K^+, Mg^{2+} and Sr^{2+} were determined by ICP optical emission spectrometry. The anion concentrations of SO_4^{2-} and Cl^- were determined by ion chromatography (Dionex ICS-90) (Banks and Frengstad, 2006; Zhao et al., 2010).

4.2. Measurements of stable isotopic compositions of oxygen ($\delta^{18}O$), hydrogen (δ^2H) and carbon ($\delta^{13}C$)

Water samples for $\delta^{18}O$ and δ^2H analysis were collected in 60 ml hydroplastic bottles. During the collecting process the bottles were completely filled with water to prevent any evaporation, and stored in a refrigerator until further analysis. $\delta^{18}O$ and δ^2H analysis was by conventional laser absorption spectroscopy in a liquid-water isotope analyzer (Los Gatos Research, Inc, USA). The $^{18}O/^{16}O$ and $^2H/^1H$ were expressed in the δ notation as parts/thousand differences (‰) with respect to the Vienna Standard Mean Ocean Water (VSMOW). The resolution of the $\delta^{18}O$ and δ^2H measurements were 0.07‰ and 0.2‰ respectively.

Water samples for $\delta^{13}C_{DIC}$ analysis were collected in 600 ml hydroplastic bottles. All inorganic dissolved carbon was precipitated as $BaCO_3$ by the NaOH–$BaCl_2$ method *in situ* (Liu et al., 2003). The $BaCO_3$ was analyzed in the laboratory with a GV IsoPrim IRMS. The carbon isotope data refer to the composition of the dissolved inorganic carbon (DIC) and are given as per mil (‰) deviations from the PDB standard; the standard deviation (1σ) was 0.15‰.

4.3. Calculation of CO_2 partial pressure and the calcite saturation index

The CO_2 partial pressure (pCO_2) and calcite saturation index (SIc) of karst water were calculated with PHREEQC (Parkhurst and Appelo, 1999) using the physicochemical data, including water temperature, pH, concentrations of Ca^{2+} and HCO_3^- (*in situ*), and the laboratory analyses of K^+, Na^+, Mg^{2+}, Cl^-, SO_4^{2-} concentrations.

4.4. Calculation methods of karst-related carbon sink

This section includes two steps; first, calculation of proportion of glacier meltwater infiltrating into the JDSM karst aquifer by use of a stable isotopic ($\delta^{18}O$, δ^2H) mixing equation and, second, estimation of the karst-related carbon sink. Fig. 6 illustrates our method of estimating the proportion of glacier meltwater in aquifer. In this section, some important formulae will be introduced.

Relevant chemical, isotopic and hydrological data must be collected before the calculation. These are δ_A, δ_B, δ_{mix}, α, C_A, C_B, C_{mix}, *and P*, where δ_A is the stable isotopic ratio in the glacier meltwater ($\delta^{18}O$ or δ^2H, unit: ‰); δ_B is the stable isotopic ratio in similar infiltration water on non-glacier covered mountain ($\delta^{18}O$ or δ^2H, unit: ‰); δ_{mix} is the stable isotopic ratio of mixtures of glacier meltwater and non-glacial groundwater ($\delta^{18}O$ or δ^2H, unit: ‰); α is the effective infiltration coefficient of precipitation before climate warming in the study region ($\alpha = I/P$); C_A is the bicarbonate concentration of extra glacier meltwater under climate warming (mmol/L); C_B is the bicarbonate concentration of similar spring water from non-glacier covered mountain (mmol/L); C_{mix} is the bicarbonate concentration of glacier meltwater mixed with non-glacial groundwater (mmol/L); and P is the precipitation in the study area (mm).

The equation for the calculation is:

$$\delta_{mix} = R_A \times \delta_A + (1 - R_A) \times \delta_B \quad (1)$$

where R_A is the proportion of extra glacier meltwater in spring water of a snow mountain. It is defined as $R_A = \Delta I/(I + \Delta I)$, where I

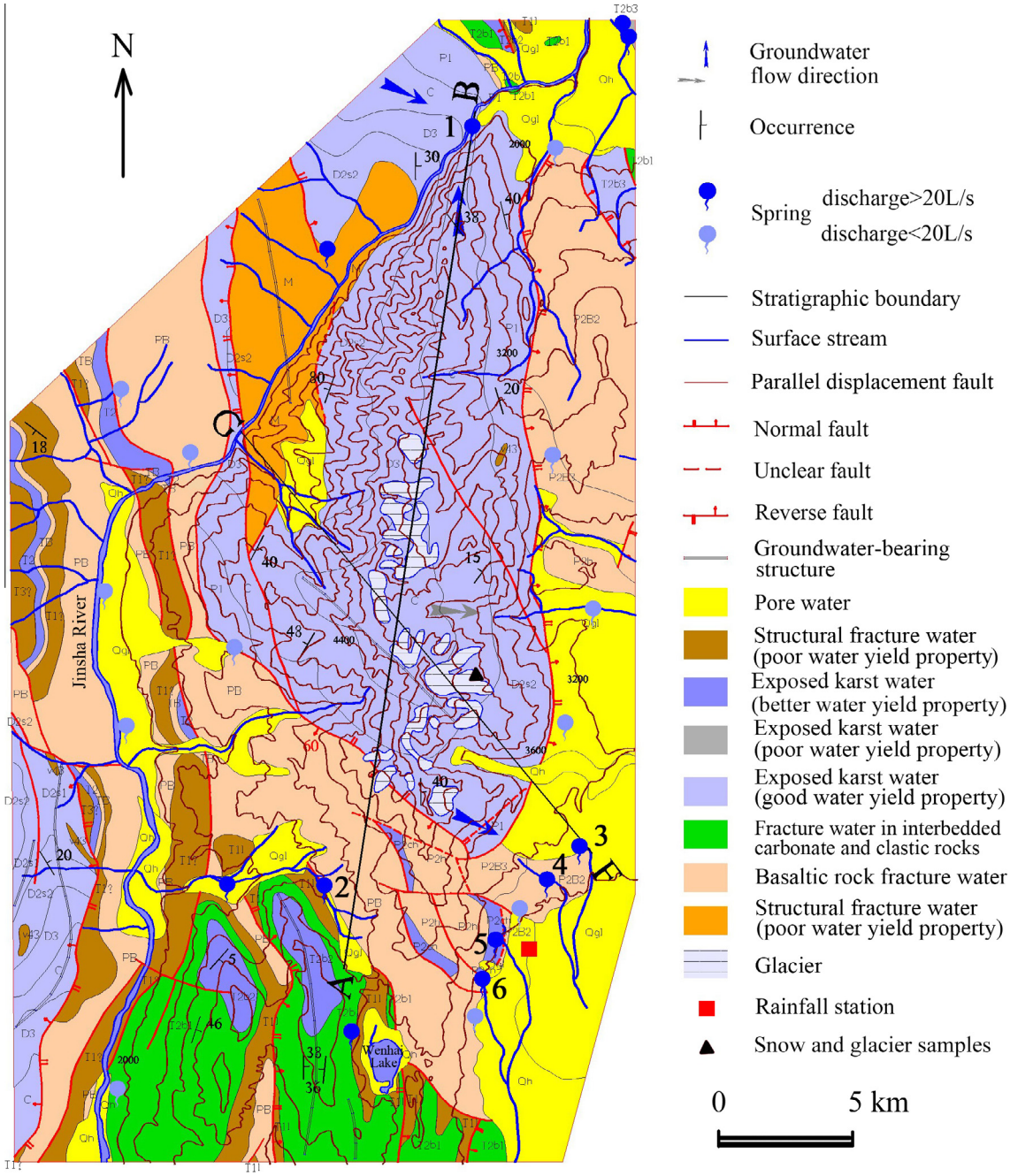

Fig. 3. Sketch hydrogeological map of the study area in the Jade Dragon Snow Mountain region (The names of the studied springs are the same as those in Fig. 1).

is the infiltration of effective precipitation; ΔI is the infiltration of extra glacier meltwater during climate warming. $\Delta I = I \times R_A/(1 - R_A)$ can be yielded by the definition of R_A.

Under climate warming, the snow line retreats upward and a large amount of previously solid glacier ice is converted into liquid water that penetrates the underlying aquifer. The glacial mass balance is adapting to new conditions. The new infiltration coefficient for precipitation in the snow mountain region can be estimated:

$$\alpha' = (I + \Delta I)/P = I/[P(1 - R_A)] = \alpha/(1 - R_A) \quad (2)$$

$$M = \alpha' \times P \quad (3)$$

where M is the new runoff modulus in snow mountain area.

According to Liu et al. (2010), the carbonate weathering (karst)-related carbon sink flux can be calculated as

$$\mathrm{CSF} = 0.5 \times M \times C_{mix} \times 44 \quad (4)$$

The factor 0.5 results from the fact that in the case of carbonate dissolution ($CaCO_3 + CO_2 + H_2O \rightarrow Ca^{2+} + 2HCO_3^-$) only half of the ($HCO_3^-$) is of atmospheric origin (i.e. the carbon sink).

The CSF equation can be transformed into:

$$\mathrm{CSF} = 22\alpha P C_{mix} \frac{\delta_A - \delta_B}{\delta_A - \delta_{mix}} \quad (5)$$

Let $x_1 = \delta_A$, $x_2 = \delta_B$, $x_3 = \delta_{mix}$, $x_4 = C_{mix}$, $E = 22\alpha P$, $y = \mathrm{CSF}$, According to the relevant error analysis theory, the root mean square error (RMSE) of CSF can be estimated by

$$m_y = \sqrt{\left(\frac{\partial y}{\partial x_1}\right)^2 m_1^2 + \left(\frac{\partial y}{\partial x_2}\right)^2 m_2^2 + \left(\frac{\partial y}{\partial x_3}\right)^2 m_3^2 + \left(\frac{\partial y}{\partial x_4}\right)^2 m_4^2} \quad (6)$$

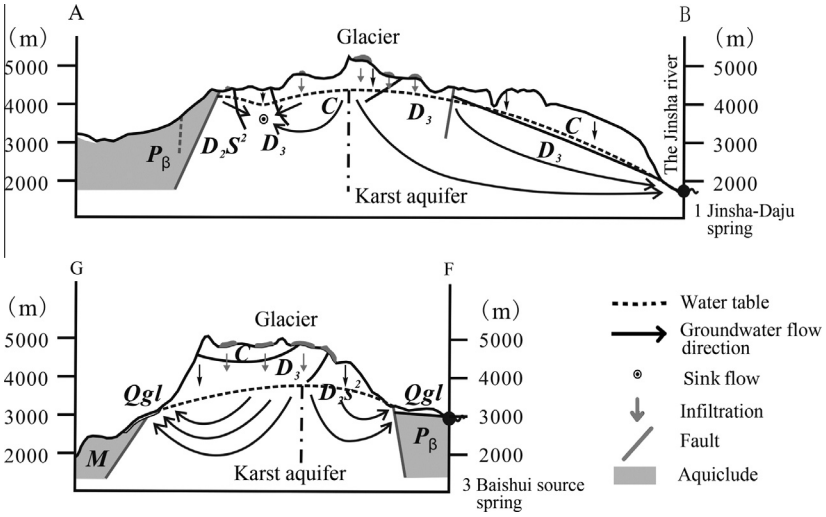

Fig. 4. Cross-sections of the Jade Dragon Snow Mountain karst aquifer. D_2S^2: Sanxiangu Formation, middle Devonian; D_3: marble and dolomitic marble, upper Devonian; C: crystalline limestone and marble, Carboniferous; P_β: volcanic tuff, Permian; *Qgl*: Quaternary unconsolidated glacial till; M: metamorphic rock (sericitic schist).

where

$$\frac{\partial y}{\partial x_1} = E\frac{(x_2 - x_3)x_4}{(x_1 - x_3)^2}$$

$$\frac{\partial y}{\partial x_2} = E\frac{-x_4}{x_1 - x_3}$$

$$\frac{\partial y}{\partial x_3} = E\frac{(x_1 - x_2)x_4}{(x_1 - x_3)^2}$$

$$\frac{\partial y}{\partial x_4} = E\frac{x_1 - x_2}{x_1 - x_3}$$

m_1, m_2, m_3, m_4 are the root mean square errors of δ_A, δ_B, δ_{mix}, C_{mix} respectively.

5. Results

The results of this work are presented in statistical tables (Table 1) and Figs. 7–9.

5.1. Hydrochemistry of the spring waters surrounding the Snow Mountain

5.1.1. Major and minor ions and Calcite Saturation Indices

In Fig. 7 the major ions of the groundwater samples are plotted onto a Piper diagram. All of these springs are simple HCO_3–Ca waters. However, the concentrations of Na^+ and K^+ at the Yushuizhai spring (6) are relatively higher than other springs (Table 1) due to its longest flow path and thus longest water–rock interaction.

Water temperatures of these springs surrounding Jade Dragon Snow Mountain ranged between 6.50 and 13.64 °C. Baishui Spring (3) had the lowest water temperature (mean value of 8.96 °C) among the southeastern springs.

The concentration of SiO_2 in the springs follows the sequence Yushuizhai Spring (6) > Heishui Spring (4) > Changshui Spring (2) > Yuzhuqingtian Spring (5) > Jinsha-Daju Spring (1) > Baishui Spring (3) (Table 1), showing that the spring with the largest proportion of silicate in its catchment has higher concentrations of SiO_2 than the more carbonate-rich catchments.

The calcite saturation indices (SI_c) of these springs range from −0.04 to 0.13 (Table 1). These values may be considered close to 0.00, indicating that they are close to equilibrium calcite dissolution/precipitation in these aquifers.

5.1.2. Stable isotopic patterns

The $\delta^{18}O$ and δ^2H values of the springs range from −15.79‰ to −14.37‰ and from −114.80‰ to −103.45‰ respectively (Table 1). It is clearly seen that Baishui Spring (3) has the heaviest oxygen and hydrogen isotopic composition among the springs studied, although its altitude is greater than the other springs.

The $\delta^{18}O$ and δ^2H values of ice, snow melt water and rain water in the study area varied more widely than spring water (Fig. 8). $\delta^{18}O$ values of rain water varied between −30‰ and −5‰, and ice and snow between −20‰ and 0‰.

The spring waters had the $\delta^{13}C$-DIC values between −6.82% and −1.50‰, with the lowest for Baishui Spring (3) and the highest for Yushuizhai Spring (6) (Table 1).

5.2. Seasonal hydrological and hydrochemical variations of the southeast springs

Seasonal physicochemical data from the southeast springs are displayed in Fig. 9. However, discharge data were available only for Baishui Spring (3). As input signals for the springs, the monthly rainfall and air temperature records show distinctly subtropical monsoon climatic characteristics, i.e. clear seasonal cycles synchronized with each other. The discharge also demonstrates a cycle but it lags behind rainfall and air temperature by approximately six months, with discharge reaching a maximum in December and minimum in June.

The water temperature, pH, pCO_2, HCO_3^-, Sr/Ca ratios, δ^2H and $\delta^{13}C$ show more spatial variations than temporal changes, i.e. these indices show some temporal fluctuation, but their seasonal cycles are not so prominent (Fig. 9).

6. Discussion

6.1. The hydrochemical data and a groundwater conceptual model

There are massive amygdaloidal basalt and volcanic tuffs of Permian age on the southwest, south and northeast sides of the Snow Mountain. These volcanic rocks lack deep weathered soils

Fig. 5. (A) Southern boundary of carbonate rock and basaltic rock in the JDSM massif. (B) The Baishui No. 1 glacier at the top of the JDSM. (C) Glacial tongue of the Baishui No. 1 glacier. (D) Fissures in the bedrock underlying the glacier. (E) Corrosion fissures in the bedrock. (F) The Baishui Spring (3). (G) Dripping water in a 150 m adit near Jinsha-Daju Spring (1). (H) The Jinsha-Daju Spring (1) and the Jinsha River.

on top because of the intensive fluvial entrenchment and the severe cold alpine environment. Furthermore, diagenetic and weathering fissures have developed sparsely. As a result, the basalts as a whole have low permeability. However, there are some well-connected tectonic faults (Fig. 3) that permit significant circulation of groundwater along them. There are also some carbonate

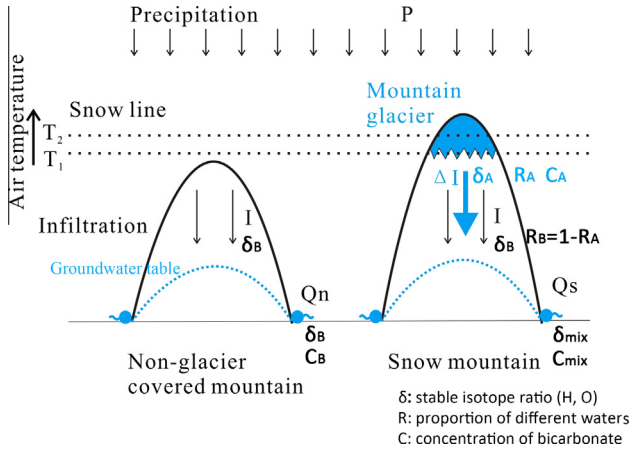

Fig. 6. Illustration of ideal "paired similar" mountain as natural pluviometer to estimate proportion of extra glacier meltwater infiltrating into aquifer by use of stable isotope data.

trap fillings in the faults. These localized faults control the local groundwater flow in the basalts. The combination of carbonate and igneous rocks controls the characteristics of the groundwater hydrochemical evolution.

The springs are of the simple HCO_3–Ca type, with low total dissolved solids, but with the minor elements and stable isotopes displaying distinct differences where the principal rock types in the aquifers feeding the springs are different. Changshui Spring (2) drains a simple basalt fracture aquifer, Heishui (4), Yuzhuqingtian (5) and Yushuizhai (6) springs belong to the basalt with carbonate trap fracture aquifer category, whereas Baishui (3) and Jinsha-Daju (1) springs belong to diffuse flow karst aquifer type (Fig. 3).

The local basalt is composed of plagioclase, pyroxene, olivine and other silicate minerals. Incongruent weathering of anorthite and albite in CO_2-enriched waters yields Na^+–HCO_3^- and SiO_2 solutions (Alemayehu et al., 2011); thus, the weathering of silicate minerals in the basalt aquifer determines the concentration of Na^+ and SiO_2 in spring waters. The carbonate rocks consist of calcite and dolomite, and their weathering usually results in Ca^{2+}, Mg^{2+}–HCO_3^- solutions. Consequently, the Na^+ and SiO_2 contents of the Yuzhuqingtian (5), Yushuizhai (6), Changshui (2) and Heishui (4) spring waters are higher than those of Baishui Spring (3) (Table 1).

The dissolution rate of carbonate is much higher than silicate (Liu et al., 2011). The Ca^{2+} and HCO_3^- concentrations of Heishui (4), Yuzhuqingtian (5) and Yushuizhai (6) springs are higher than that of Changshui Spring (3) because of water–rock interaction between fault groundwater and the carbonate rock trap in the water-transmitting faults.

The relationship between Sr/Ca ratios and EC illustrates the different aquifers supplying these springs. Weathering of silicate minerals usually produces high Sr/Ca ratios, while low Sr/Ca ratios are associated with the dissolution of calcium carbonate (Wiegand, 2009). The differences between Sr/Ca ratios and EC at the springs is large (Fig. 10). The Sr/Ca ratio of the Baishui Spring (3) is the lowest of all, indicating that it is simple karst water. The Sr/Ca ratios of the Heishui (4), Yushuizhai (6), Yuzhuqingtian (5), and Changshui (2) springs are higher than that of Baishui (3), because the former are from silicate fracture aquifers. Although it is a karst spring, Jinsha-Daju (1) shows a relatively high Sr/Ca ratio, because it belongs to the regional flow system of the JDSM karst aquifer with admixture of some water from the basalt aquifer. In addition, the spring is close to the Jinsha River (the modern karst drainage base level of the JDSM alpine karst aquifer) and its long flow path extends the time of water and rock interaction (Wang et al., 2003) and thus increases the conductivity of spring water (Table 1).

As a result, there are four categories of springs: Baishui Spring (3) is fed mainly by the JDSM carbonate aquifer, Changshui Spring (2) is supplied mainly by the JDSM southern silicate aquifer, Heishui (4) and Yuzhuqingtian (5) springs are influenced by carbonate rock traps although they are located in the basalt aquifer, while Jinsha-Daju (1) and Yushuizhai (6) springs are supplied by both carbonate and basalt aquifers.

The stable oxygen and hydrogen isotope compositions show differences too. The groundwater sources can be identified from them. The local meteoric water line is plotted in Fig. 8. The δ^2H and $\delta^{18}O$ values of rainfall range from −220‰ to −50‰ and −30‰ to −7‰, respectively, reflective of the strong monsoonal behavior. The δ^2H and $\delta^{18}O$ values of snow and ice melt water range from −160‰ to 20‰ and −20‰ to 0‰, respectively. However, the δ^2H and $\delta^{18}O$ values of all springs are concentrated in a narrow central (average) zone (Fig. 8), indicating the strong regulating and storage functions of groundwater in these aquifers. The isotope data clearly indicate that the spring waters are of entirely meteoric origin.

Fig. 11 further emphasizes the isotopic differences among the springs. The elevation of Baishui Spring (3) is greater than all others except Heishui Spring (4), yet its δ^2H and $\delta^{18}O$ values are the heaviest. The distinct isotope compositions of Baishui Spring (3) are most probably produced by glacier melt water (with heavier isotopes) which recharges the underlying karst aquifer (Figs. 3 and 4).

Generally speaking, the δ^2H and $\delta^{18}O$ values of precipitation over mountains display strong altitudinal depletion, i.e., the δ^2H and $\delta^{18}O$ values of precipitation decrease with increasing altitude (He et al., 2001; Pang, 2006; Pu et al., 2013b). However, the δ^2H and $\delta^{18}O$ values of snow and ice melt water at the top of the Snow Mountain are heavier than rainfall (Fig. 8). This phenomenon can be attributed to processes of sublimation and vapor exchange which have happened at the surface and inside the glacier and snow pack, favoring the enrichment of old snow in δ^2H and $\delta^{18}O$ (Clark and Fritz, 1997; Pang et al., 2006). This finding gives an effective way to calculate the proportion of glacier melt water infiltrating into the underlying karst aquifer.

A conceptual hydrogeological model of the JDSM alpine karst aquifer of Baishui Spring (3) is proposed in Fig. 12. The mountain can be divided into two horizontal and two vertical zones based on bedrock type and glacier cover. Horizontally there is the glacier-influenced carbonate diffuse flow aquifer and the non-glacierized basalt fracture aquifer. The two vertical zones are the cryosphere above and normal rainfall zone below the snow line. The glacier accumulation zone covers the mountaintop karst aquifer. There is a generally thick unsaturated zone between the glacier and saturated zone (watertable) in the carbonate mountain. There is a mixing area (rain water and glacier melt water) in the discharge area near the karst spring. The stable oxygen and hydrogen isotope composition of rain water are characterized by altitude effects, but those of glacier melt water show heavier values. Glacier melt water moves downward and mixes with rainwater-sourced groundwater in the discharge area.

The time lag between peak seasonal precipitation and air temperatures and the discharge at Baishui Spring (3) is about six months (Fig. 9). The thick unsaturated zone increases the amount of time for infiltration of the large amounts of glacier melt water produced in summer to reach the water table, and the diffuse-flow nature of the fissured carbonate aquifer further delays the transmission of groundwater. These features of the glacier-covered alpine karst aquifer control the hydrochemical

Table 1
Annual mean value and coefficient of variation of physicochemical parameters of spring water samples around the Jade Dragon Snow Mountain.

Item	Unit	Jinsha-Daju Spring (1)	Changshui Spring (2)	Baishui Spring (3) (n = 14)				Heishui Spring (4) (n = 14)				Yuzhuqingtian Spring (5) (n = 14)				Yushuizhai Spring (6) (n = 13)			
		Jan 17, 2014	Dec 12, 2013	Mean	Max	Min	Cv	Mean	Max	Min	Cv	Mean	Max	Min	Cv	Mean	Max	Min	Cv
Temp	°C	11.70	6.50	8.96	9.20	8.80	0.01	10.46	11.70	10.00	0.04	10.11	10.60	9.80	0.02	13.64	17.30	11.30	0.11
pH		7.74	8.28	7.88	8.05	7.66	0.01	8.13	8.44	7.88	0.02	8.06	8.32	7.64	0.02	7.76	7.88	7.63	0.01
K^+	mg/L	0.15	0.07	0.08	0.09	0.04	0.17	0.22	0.32	0.13	0.23	0.21	0.35	0.11	0.35	0.70	0.91	0.55	0.16
Na^+	mg/L	1.17	0.83	0.23	0.33	0.14	0.23	0.76	0.93	0.53	0.15	0.94	1.13	0.84	0.09	5.22	6.06	3.75	0.11
Ca^{2+}	mg/L	48.00	27.00	45.29	48.00	42.00	0.04	37.50	41.00	34.00	0.05	37.29	40.00	34.00	0.04	51.77	64.00	38.00	0.13
Mg^{2+}	mg/L	7.57	2.55	4.13	5.97	3.21	0.20	3.66	5.42	1.54	0.32	4.69	6.33	3.62	0.23	6.41	6.87	5.90	0.06
Cl^-	mg/L	0.70	0.13	0.25	0.41	0.15	0.28	0.14	0.19	0.08	0.25	0.35	0.70	0.14	0.36	1.07	1.34	0.87	0.10
SO_4^{2-}	mg/L	8.20	1.54	1.00	1.22	0.69	0.16	1.81	2.52	1.11	0.21	4.60	5.55	3.87	0.12	8.36	9.49	6.94	0.08
HCO_3^-	mg/L	161.64	79.30	136.37	140.30	134.19	0.02	109.36	115.90	97.59	0.04	110.67	115.90	109.80	0.02	170.33	183.00	146.38	0.05
SiO_2	mg/L	2.77	5.36	1.31	1.43	1.17	0.06	6.15	6.64	5.42	0.06	3.92	4.42	3.42	0.07	7.11	8.35	6.22	0.09
Sr^{2+}	mg/L	0.12	0.09	0.04	0.04	0.03	0.10	0.09	0.09	0.07	0.08	0.08	0.09	0.08	0.05	0.21	0.24	0.15	0.09
EC	μs/cm	270.00	128.00	208.08	221.00	199.10	0.03	170.82	183.30	162.90	0.03	178.93	181.80	175.40	0.01	275.23	286.00	226.00	0.05
pCO_2	Pa	245.47	33.19	149.49	239.88	100.93	0.27	71.82	118.03	34.51	0.37	86.46	208.93	42.85	0.47	252.37	352.37	100.00	0.26
SI_C		0.02	−0.04	0.04	0.22	−0.21		0.13	0.51	−0.14		0.06	0.32	−0.39		0.11	0.31	−0.07	
$\delta^{18}O$	‰	−15.66	−15.79	−14.37	−13.62	−14.74		−14.86	−14.26	−15.45		−15.17	−14.89	−15.43		−15.22	−14.81	−15.46	
$\delta^{2}H$	‰	−112.87	−114.80	−103.45	−100.70	−104.96		−108.05	−106.40	−109.33		−109.34	−108.03	−110.26		−110.56	−109.48	−111.29	
$\delta^{13}C$	‰	−2.39	−2.57	−6.82	−2.77	−9.53	−0.26	−4.96	1.25	−8.44	−0.51	−3.72	0.38	−7.22	−0.52	−1.50	1.62	−2.60	−0.75
Altitude	m	1620	2795	2866				2869				2766				2741			

Cv (coefficient of variation = standard deviation/mean). Cv are not reported for saturation index of calcite and dolomite because these values can be positive and negative.

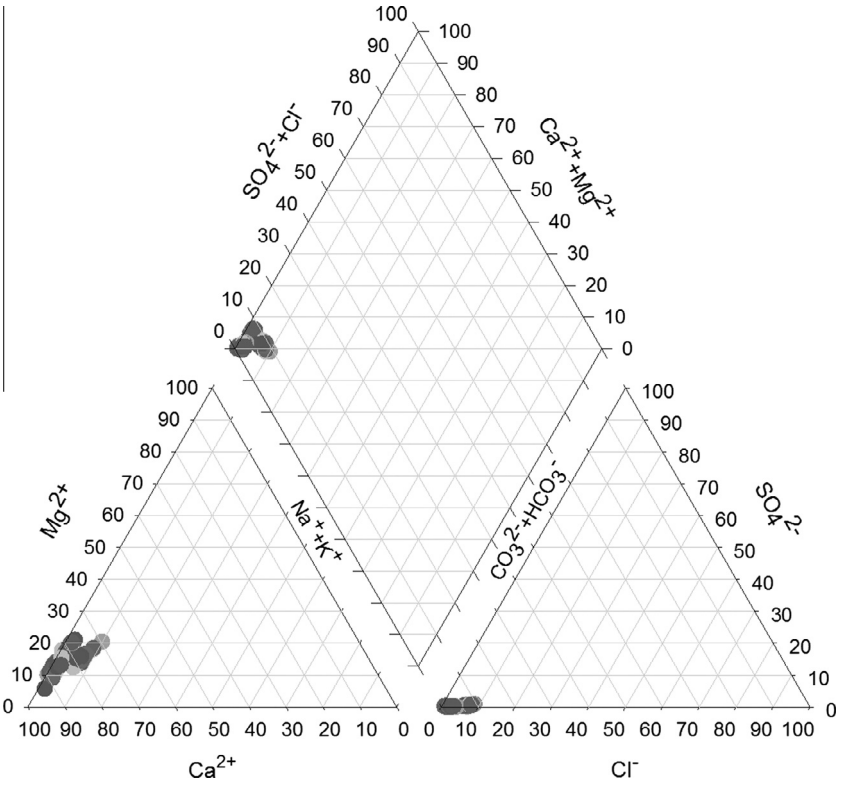

Fig. 7. Piper diagram of the spring waters around the snow mountain karst aquifer.

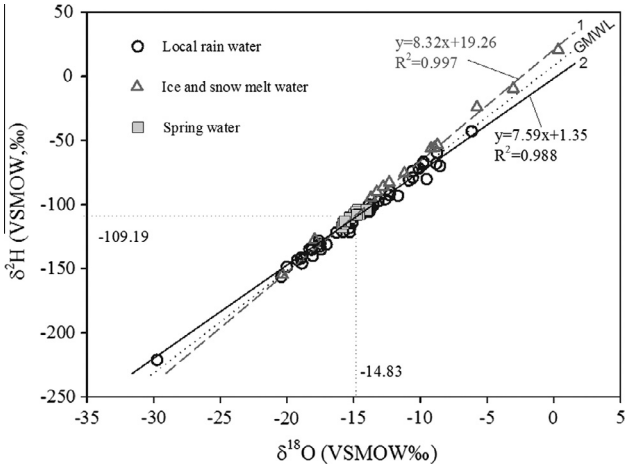

Fig. 8. $\delta^{18}O$ and $\delta^{2}H$ values of rainwater, ice and snow melt water, and spring water in the study area. 1: for ice and snow melt water; 2: for rainwater; GMWL: Global Meteoric Water Line.

and isotopic variations, for instance, HCO_3^-, Sr/Ca, δ^2H, $\delta^{13}C$, etc. are relatively stable (Fig. 9).

6.2. Calculation of the karst related carbon sink flux of the Baishui Spring (3) catchment

As mentioned above, there are lots of discharge areas surrounding the JDSM alpine karst aquifer. Large quantities of karst groundwater discharge laterally through the eastern porous aquifer overlying the basalt basement rock. It is difficult to calculate the flux of the karst-related carbon sink by a solute load method because of the difficulty in determining the karst catchment area and the overall quantity of groundwater discharge. Fortunately, Baishui Spring (3) gives important hydrochemical information about the JDSM karst aquifer water contributing to the eastern porous aquifer. The spring is an overflow spring because of the low permeability of the underlying basalt with (Fig. 4). We can use the δ^2H and $\delta^{18}O$ data of the spring to calculate the mixing proportion of glacier melt water recharging the groundwater, based on the conceptual hydrogeological model as shown in Figs. 6 and 12.

In the JDSM region, the large and rugged landforms and mountain microclimate effects make it impossible to deploy a large number of rainfall collectors on mountain tops to obtain valid rainfall isotope information. However, we can use the springs which have similar aquifers as natural pluviometers to inversely calculate the stable oxygen and hydrogen isotopic compositions of rainfall (Minissale and Vaselli, 2011). Part A and Part C in Fig. 12 have similar topography and rainwater-catchment areas, so they probably have the same δ^2H and $\delta^{18}O$ precipitation values. Part A aquifer can be seen as similar to the catchment of Part C. Accordingly, the carbonate aquifer covered with glacier ice has two ^{18}O and ^{2}H end-members. One end-member is represented by glacier melt water (δ_A), and the other is the rainfall-recharged aquifer, here represented by Yushuizhai Spring (6) (δ_B) (Table 2). Therefore, the mixing proportion of glacier melt water in the Baishui Spring (3) (R_A) can be inversely calculated by a stable isotope mixing equation using δ^2H and $\delta^{18}O$ values of the two end-members (Table 2) by Eq. (1) in Section 4.4. It is about 29.34%.

The concentration of HCO_3^- in Baishui Spring (3) is 136.37 mg/L, while that of glacier melt water is 24.4 mg/L (measured *in situ*). It can be inversely calculated that the HCO_3^- content of spring water will be 182.9 mg/L if any mixing effect is neglected.

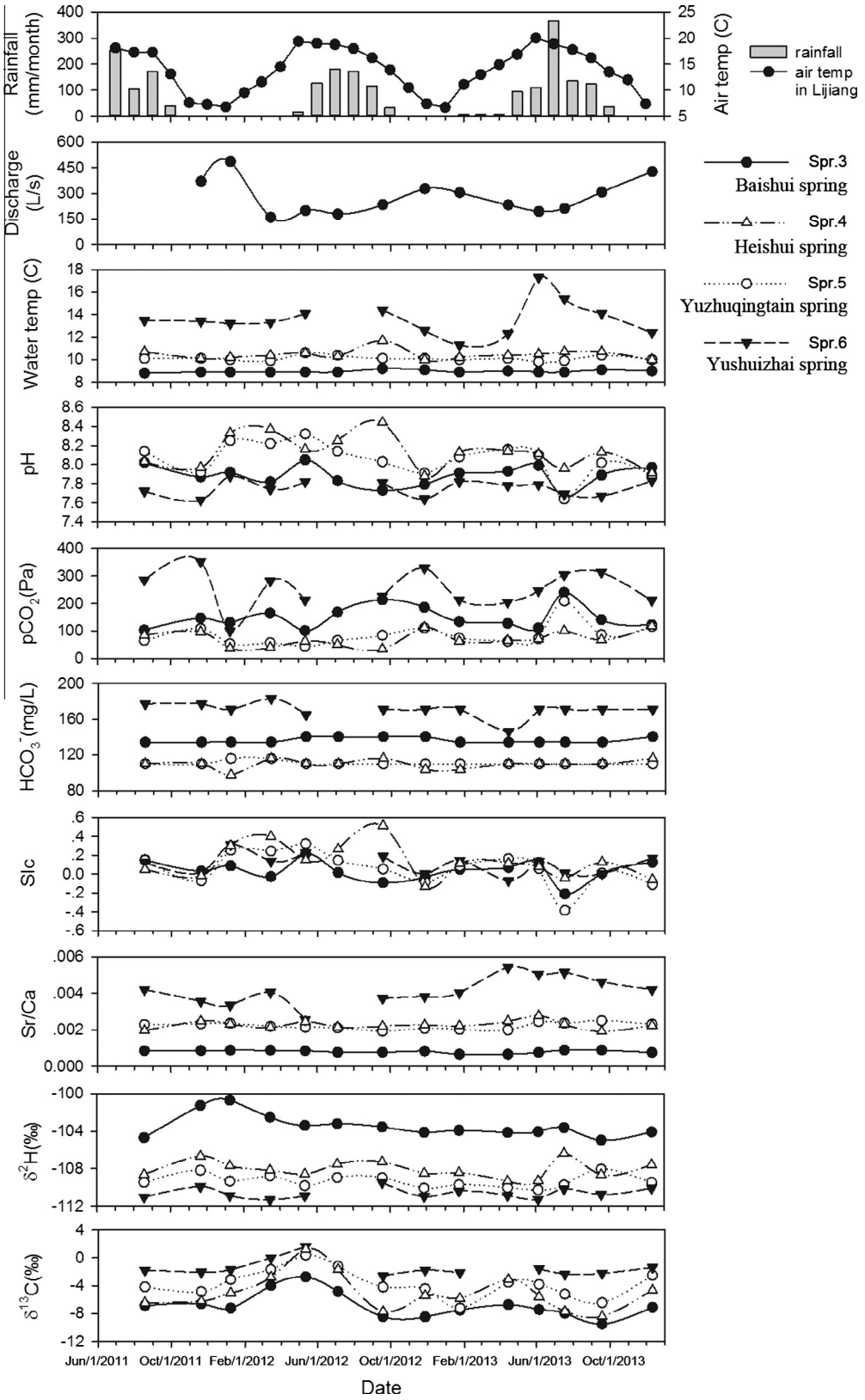

Fig. 9. Seasonal hydrological and hydrochemical variations of the southeastern springs.

The effective infiltration coefficient of the carbonate mountain massif in the Lijiang Basin is 0.4 (Li et al., 1979). By using the calculated value of mixing contributions, the infiltration coefficient (α) of precipitation and extra glacier melt water produced by the present climate warming scenario can be calculated.

$$\alpha = 0.4 \times 1/(1 - 29.34\%) = 0.5661$$

The annual average precipitation (P) of the Lijiang district is 957.2 mm. Therefore, the runoff modulus (M) of the Baishui Spring (3) catchment is:

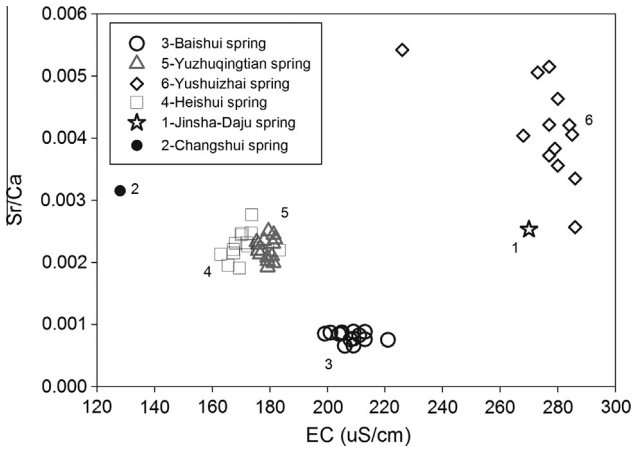

Fig. 10. Sr/Ca ratios versus EC of spring waters.

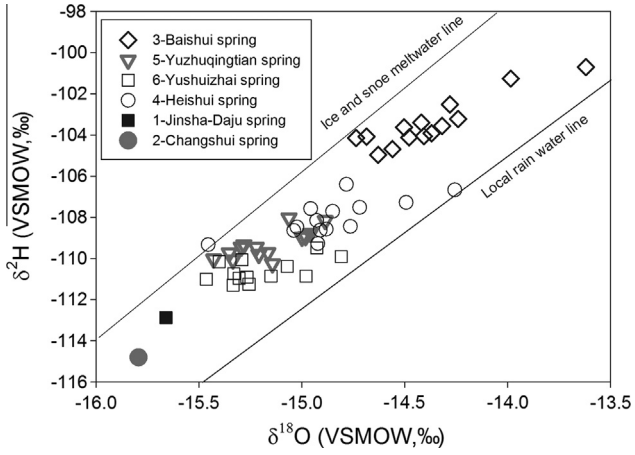

Fig. 11. Relationship between δ^2H and $\delta^{18}O$ values of spring waters.

$$M = \alpha \times P \times 10^6 (L\,km^{-2}\,a^{-1}) = 0.5661 \times 957.2 \times 10^6 = 5.42 \times 10^8 (L\,km^{-2}\,a^{-1})$$

According to Liu et al. (2010), the karst-related carbon sink flux (CSF) can be calculated by Eq. (4), as:

$$CSF = 0.5 \times M \times [HCO_3^-] \times 44 = 0.5 \times 5.42 \times 10^8 \times 136.37/61 \times 44 (mg\,km^{-2}\,a^{-1}(CO_2)) = 26.65 t\,km^{-2}\,a^{-1}(CO_2)$$

The CSF and its root mean square error can also be calculated by Eqs. (5) and (6), respectively. Here we give the outcomes of CSF by use of δ^2H and $\delta^{18}O$ values respectively.

By using δ^2H value:

$$CSF = 27.39 \pm 6.59\ t\,km^{-2}\,a^{-1}(CO_2)$$

By using $\delta^{18}O$ value:

$$CSF = 25.95 \pm 3.44\ t\,km^{-2}\,a^{-1}(CO_2)$$

The average CSF is $26.67 \pm 3.44\ t\,km^{-2}\,a^{-1}(CO_2)$, which is almost the same as that yielded by Eq. (4).

6.3. Comparison with carbonate and non-carbonate catchments elsewhere in the world

The calculated karst related carbon sink flux of the Baishui Spring (3) aquifer is 26.65 t km^{-2} a^{-1} as CO_2. This is lower than that of the Tsanfleuron glacierized alpine karst aquifer influenced more strongly by the global warming (58.96 t km^{-2} a^{-1}(as CO_2), Zeng et al., 2012), and of the Houzhai karst subterranean river catchment, a typical carbonate catchment of Southwestern China with a humid subtropical monsoon climate (44.37 t km^{-2} a^{-1}(as CO_2), Yan et al., 2012), showing the importance of climate in determining the karst-related carbon sink flux. Compared with silicate catchments, however, the carbon sink flux in karstic catchments is much higher. Results from a Susquehanna Shale Hills catchment, USA, show that silicate weathering consumes CO_2 at a rate of only

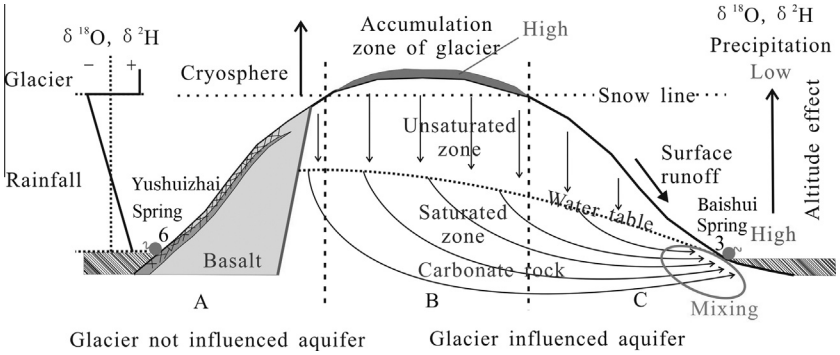

Fig. 12. Conceptual hydrogeological model of the glacier-influenced and not influenced components of the aquifer supplying Baishui Spring (3).

Table 2
Parameters of oxygen and hydrogen isotopic compositions to calculate proportion of glacier melt water recharge into the alpine karst groundwater flow system of Baishui Spring (3).

Name of sample	Number of samples	Mean of $\delta^{18}O$	Root mean square error	Mean of δ^2H	Root mean square error
Yushuizhai Spring (6)	13	−15.22‰	0.19‰	−110.56‰	0.53‰
Glacier melt water	5	−12.50‰	1.04‰	−84.64‰	7.78‰
Baishui Spring (3)	14	−14.37‰	0.28‰	−103.45‰	1.17‰
Mixing proportion of glacier melt water in Baishui Spring (3) (R_A)		31.25%		27.43%	
Mean R_A			29.34%		

1.94 t km^{-2} a^{-1} (Jin et al., 2014). The silicate weathering carbon sink is only 7.3% of the karst sink flux in this comparison, emphasizing the control of lithology on the rock weathering-related carbon sink.

7. Conclusions

Hydrogeological survey together with natural hydrochemical and stable isotopic tracers were successfully applied to establish a karst hydrogeological model for the Jade Dragon Snow Mountain region in Lijiang district, Yunnan Province, Southwestern China. Baishui Spring (3) is a good representative of the hydrogeological characteristics of the JDSM alpine karst aquifer. The stable oxygen and hydrogen isotope composition indicate that the spring waters originate from meteoric precipitation. Natural chemical tracers show that the Changshui (2), Heishui (4), Yuzhuqingtian (5) and Yushuizhai (6) springs derive from the southern JDSM basalt plus carbonate trap fracture aquifer, while the Baishui (3) and Jinsha-Daju Spring (1) waters are from the JDSM alpine carbonate karst aquifer.

There is a groundwater divide in the JDSM karst aquifer that is difficult to locate. From δ^2H and δ^{18}O values it is calculated that glacier melt water accounts for about 29.34% of the groundwater discharged at Baishui Spring (3). The karst-related carbon sink of the spring aquifer is 26.65 t km^{-2} a^{-1}(as CO_2). This is lower than that of an example of non-glacierized humid subtropical karst catchments, but over ten times higher than that of a neighboring silicate catchment, showing the control of both climate and lithology on the rock weathering-related carbon sink and the significance of carbonate weathering in the global carbon cycle.

Acknowledgments

This work was supported by the 973 Program of China (2013CB956703), and the National Natural Science Foundation of China (41430753, 41003056). Special thanks are given to Derek Ford for his thoughtful comments and suggestions, which greatly improved the original draft.

References

Alemayehu, T., Leis, A., Eisenhauer, A., Dietzel, M., 2011. Multi-proxy approach (^{2}H/H, ^{18}O/^{16}O, ^{13}C/^{12}C and ^{87}Sr/^{86}Sr) for the evolution of carbonate-rich groundwater in basalt dominated aquifer of Axum area, northern Ethiopia. Chem. Erd. 71, 177–187.

Anderson, S.A., Drever, J.I., 1997. Humphrey N F. Chemical weathering in glacial environments. Geology 25, 399–402.

Banks, D., Frengstad, B., 2006. Evolution of groundwater chemical composition by plagioclase hydrolysis in Norwegian anorthosites. Geochim. Cosmochim. Acta 70, 1337–1355.

Clark, I., Fritz, P., 1997. Environmental isotopes in hydrogeology. Lewis publishers, Boca Raton, FL. Cooper, L.W., 1998. Isotopic fractionation in snow cover. In: Kendall, C., McDonnell, J.J. (Eds.), Isotope Tracers in Catchment Hydrology. Elsevier, pp. 119–136 (Chapter 4).

Du, J.K., Xin, H.J., He, Y.Q., Niu, H.W., Pu, T., Cao, W.H., Zhang, T., 2013. Response of modern monsoon temperate glacier to climate change in Yulong Mountain. Sci. Geogr. Sin. 33, 890–896 (In Chinese with English abstract).

Fetter, C.W., 1994. Applied Hydrogeology. Macmillan college publishing company, New York, pp. 401–407.

Gibbs, M.T., Kump, L.R., 1994. Global chemical erosion during the last glacial maximum and the present: sensitivity to changes in lithology and hydrology. Paleoceanography 9, 529–543.

Gleick, P.H., 1996. Water resources. In: Schneider, S.H. (Ed.), Encyclopedia of Climate and Weather, vol. 2. Oxford University Press, New York, pp. 817–823.

Gremaud, V., Goldscheider, N., Savoy, L., Favre, G., Masson, H., 2009. Geological structure recharge processes and underground drainage of a glacierized karst aquifer system, Tsanfleuron-Sanetsch, Swiss Alps. Hydrogeol. J. 17, 1833–1848.

Hartmann, A., Goldscheider, N., Wagener, T., Lange, J., Weiler, M., 2014. Karst water resources in a changing world: review of hydrological modeling approaches. Rev. Geophys. 52, 218–242.

He, Y.Q., Theakstone, W.H., Yao, T.D., Shi, Y.F., 2001. The isotopic record at an alpine glacier and its implications for local climatic changes and isotopic homogenization processes. J. Glaciol. 47, 147–151.

He, Y.Q., Yao, T.D., Theakstone, W.H., Chen, T., Zhang, D.D., 2002. The irregular pattern of isotopic and ionic signals in the typical monsoon temperate-glacier area, Yulong Mountain, China. Ann. Glaciol. 35, 167–174.

He, Y.Q., Zhang, Z.L., Theakstone, W.H., Chen, T., Yao, T.D., Pang, H.X., 2003. Changing features of the climate and glaciers in China's monsoonal temperate glacier region. J. Geophys. Res. 108, ACL1.1–ACL1.7.

He, Y.Q., Gu, J., 2003. What is the major reason for glacier retreat on Yulong Mountain, China? J. Glaciol. 49, 325–326.

He, Y.Q., Pang, H.X., Theakstone, W.H., Zhang, D.D., Lu, A.G., Song, B., Yuan, L.L., Ning, B.Y., 2006. Spatial and temporal variations of oxygen isotopes in snowpacks and glacial runoff in different types of glacial area in western China. Ann. Glaciol. 43, 269–274.

Huang, B.J., Zhang, Z.G., Chen, W.H., Gao, M.G., 1995. Tracing test in alpine-gorge area: a case study of Jinping District, west Sichuan. China. Carsol. Sin. 14, 362–371 (In Chinese with English abstract).

IPCC, 2013: Climate Change 2013: The physical science basis. contribution of working group i to the fifth assessment report of the intergovernmental panel on climate change. In: Stocker, T.F., Qin, D., Plattner, G.-K., Tignor, M., Allen, S.K., Boschung, J., Nauels, A., Xia, Y., Bex, V., Midgley, P.M. (Eds.), Cambridge University Press, Cambridge, United Kingdom and New York, NY, USA, 1535pp.

Jin, L., Ogrinc, N., Yesavage, T., Hasenmueller, E.A., Ma, L., Sullivan, P.L., Kaye, J., Duffy, C., Brantley, S.L., 2014. The CO_2 consumption potential during gray shale weathering: insights from the evolution of carbon isotopes in the Susquehanna Shale Hills critical zone observatory. Geochim. Cosmochim. Acta 142, 260–280.

Kääb, A., Paul, F., Maisch, M., Hoelzle, M., Haeberli, W., 2002. The new remote-sensing-derived Swiss glacier inventory: II. First results. Ann. Glaciol. 34, 362–366.

Khromova, T.E., Dyurgerov, M., Barry, R.G., 2003. Late-twentieth century changes in glacier extent in the Ak-shirak Range, Central Asia, determined from historical data and ASTER imagery. Geophys. Res. Lett. 30, 1863. http://dx.doi.org/10.1029/2003GL017233.

Kong, P., Fink, D., Na, C.G., Xiao, W., 2010. Dip-slip rate determined by cosmogenic surface dating on a Holocene scarp of the Daju fault, Yunnan, China. Tectonophysics 493, 106–122.

Krawczyk, W.E., Bartoszewski, S.A., 2008. Crustal solute fluxes and transient carbon dioxide drawdown in the Scottbreen Basin, Svalbard in 2002. J. Hydrol. 362, 206–219.

Li, J.L., Ge, Z.Y., Li, X.D., Liao, S.F., 1979. Report of hydrogeological survey in Lijiang District. The Chinese Liberation Army, Hydrogeological Investigation Report, 42–46.

Liu, Z., Zhang, M., Li, Q., You, S., 2003. Hydrochemical and isotope characteristics of spring water and travertine in the Baishuitai area (SW China) and their meaning for paleoenvironmental reconstruction. Environ. Geol. 44, 698–704.

Liu, Z., Li, Q., Sun, H., Wang, J., 2007. Seasonal, diurnal and storm-scale hydrochemical variations of typical epikarst springs in subtropical karst areas of SW China: soil CO_2 and dilution effects. J. Hydrol. 337, 207–223.

Liu, Z.H., Dreybrodt, W., Wang, H.J., 2010. A new direction in effective accounting for the atmospheric CO_2 budget: considering the combined action of carbonate dissolution, the global water cycle and photosynthetic uptake of DIC by aquatic organisms. Earth-Sci. Rev. 99, 162–172.

Liu, Z., Dreybrodt, W., Liu, H., 2011. Atmospheric CO_2 sink: silicate weathering or carbonate weathering? Appl. Geochem. 26, 292–294.

Ma, Z.L., Zhou, C.H., Zhang, Z.G., Huang, J.J., 2006. Tracer test to karst groundwater in Luoshuidong area, Jinping. Sichuan. Carsol. Sin. 25, 201–210 (In Chinese with English abstract).

Maher, K., Chamberlain, C.P., 2014. Hydrological regulation of chemical weathering and the geologic carbon cycle. Science 343, 1502–1503.

Ming, Q.Z., Shi, Z.T., Su, H., Dong, M., Liu, Y., 2007. A discussion on the formation of the Hutiaoxia Gorge on the Jinsha River. Trop. Geogr. 27, 40–404 (In Chinese with English abstract).

Minissale, A., Vaselli, O., 2011. Karst springs as "natural" pluviometers: constraints on the isotopic composition of rainfall in the Apennines of central Italy. Appl. Geochem. 26, 838–852.

Pang, H.X., He, Y.Q., Zhang, Z.L., Lu, A.G., Gu, J., Zhao, J.D., 2005. Origin of summer monsoon rainfall identified by delta 18O in precipitation. Chin. Sci. Bull. 50, 2761–2764.

Pang, H.X., 2006. Study on stable isotopes in waters over the temperate glacier region in South Asia. Doctoral Thesis of Cold and Arid Regions Environmental and Engineering Research Institute, Chinese Academy of Sciences (in Chinese with English abstract).

Pang, H.X., He, Y.Q., Lu, A.G., Zhao, J.D., Ning, B.Y., Yuan, L.L., Song, B., Zhang, N.N., 2006. Comparisons of stable isotopic fractionation in winter and summer at Baishui Glacier No. 1. Mt. Yulong. Acta Geogr. Sin. 61, 501–509 (In Chinese with English abstract).

Pang, H.X., He, Y.Q., Theakstone, W.H., Zhang, D.D., 2007. Soluble ionic and oxygen isotopic compositions of a shallow firn profile, Baishui glacier No. 1, southeastern Tibetan Plateau. Ann. Glaciol. 46, 325–330.

Parkhurst, D.L., Appelo, C.A.J., 1999. User's guide to PHREEQC (version 2) – a computer program for speciation, batch-reaction, one-dimensional transport and inverse geochemical calculations. U.S. Geological Survey, Water-Resources Investigations Report 99-4259.

Paul, F., Huggel, C., Kääb, A., 2004a. Combining satellite multispectral image data and a digital elevation model for mapping of debris-covered glaciers. Remote Sens. Environ. 89, 510–518.

Paul, F., Kääb, A., Maisch, M., Kellenberger, T., Haeberli, W., 2004b. Rapid disintegration of Alpine glaciers observed with satellite data. Geophys. Res. Lett. 31, L21402.

Pu, T., He, Y.Q., Zhang, T., Wu, J.K., Zhu, G.F., Chang, L., 2013a. Isotopic and geochemical evolution of ground and river waters in a karst dominated geological setting: A case study from Lijiang basin, South-Asia monsoon region. Appl. Geochem. 33, 199–212.

Pu, T., He, Y.Q., Zhu, G.F., Zhang, N.N., Du, J.K., Wang, C.F., 2013b. Characteristics of water stable isotopes and hydrograph separation in Baishui catchment during the wet season in Mt. Yulong region, south western China. Hydrol. Process. 27, 3641–3648.

Sharp, M.J., Tranter, M., Brown, G.H., et al., 1995. Rates of chemical denudation and CO_2 drawdown in a glacier-covered Alpine catchment. Geology 23, 61–64.

Shi, X.H., Wang, E.Q., Wang, G., Fan, C., 2008. Late Cenozoic uplift of the Yulong Snow Mountain (5596 m), SE Tibetan Plateau, caused by erosion and tectonic forcing. Quat. Sci. 28, 222–231 (In Chinese with English abstract).

Wang, Z.Y., Liu, J., Cui, Y.X., Wang, T., Guo, T.Y., 2003. Distribution characteristics of Sr/Mg, Sr/Ca and applications in Yanhe spring karst water system. Hydrogeol. Eng. Geol. 2, 15–19 (In Chinese with English Abstract).

Wiegand, B.A., 2009. Tracing effects of decalcification on solute sources in a shallow groundwater aquifer, NW Germany. J. Hydrol. 378, 62–71.

Xin, H.J., He, Y.Q., Zhang, T., 2013. The features of climate variation and glacier response in Mt. Yulong, Southeastern Tibetan Plateau. Adv. Earth Sci. 28 (11), 1257–1268 (In Chinese with English abstract).

Yan, J., Li, J., Ye, Q., Li, K., 2012. Concentrations and exports of solutes from surface runoff in Houzhai Karst Basin, southwest China. Chem. Geol. 304–305, 1–9.

Zeng, C., Zhao, M., Yang, R., Liu, Z.H., Gremaud, V., Goldscheider, N., 2011. Comparison of karst process-related carbon sink intensity between an alpine glaciated and snow covered karst water system and humid subtropical karst water system. Adv. Clim. Change Res. 7, 162–170 (In Chinese with English abstract).

Zeng, C., Gremaud, V., Zeng, H., Liu, Z.H., Goldscheider, N., 2012. Temperature-driven meltwater production and hydrochemical variations at a glaciated alpine karst aquifer: implication for the atmospheric CO_2 sink under global warming. Environ. Earth Sci. 65, 2285–2297.

Zeng, C., Yang, R., Yang, M.M., Hu, J.C., Wu, G.H., Fan, Y.H., 2013. Artificial neural network simulation to zero flow of the Heilongtan spring groups in Lijiang. Carsol. Sin. 32, 391–397 (In Chinese with English abstract).

Zhao, M., Zeng, C., Liu, Z., Wang, S., 2010. Effect of different land use/land cover on karst hydrogeochemistry: a paired catchment study of Chenqi and Dengzhanhe, Puding, Guizhou, SW China. J. Hydrol. 388, 121–130.

Zhu, G.F., Pu, T., He, Y.Q., Shi, P.J., Zhang, T., 2013. Seasonal variations of major ions in fresh snow at Baishui Glacier No. 1, Yulong Mountain, China. Environ. Earth Sci. 69, 1–10.

Zolotov, A.Y., Ivanov, V., Amelin, V., 2002. Methods and Tools for Analysis of Liquid Samples Comprehensive Analytical Chemistry. Elsevier, pp. 69–117 (Chapter 3).